Mechanism of the Highly Efficient Quenching of Tryptophan Fluorescence in Human γD-Crystallin†

Jiejin Chen,‡ Shannon L. Flaugh,‡ Patrik R. Callis,*,§ and Jonathan King*,‡

Department of Biology, Massachusetts Institute of Technology, Cambridge, Massachusetts 02139, and Department of Chemistry and Biochemistry, Montana State University, Bozeman, Montana 59717

Received May 18, 2006; Revised Manuscript Received July 22, 2006

ABSTRACT: Quenching of the fluorescence of buried tryptophans (Trps) is an important reporter of protein conformation. Human γD-crystallin (Hγ D-Crys) is a very stable eye lens protein that must remain soluble and folded throughout the human lifetime. Aggregation of non-native or covalently damaged Hγ D-Crys is associated with the prevalent eye disease mature-onset cataract. Hγ D-Crys has two homologous β-sheet domains, each containing a pair of highly conserved buried tryptophans. The overall fluorescence of the Trps is quenched in the native state despite the absence of the metal ligands or cofactors. We report the results of detailed quantitative measurements of the fluorescence emission spectra and the quantum yields of numerous site-directed mutants of Hγ D-Crys. From fluorescence of triple Trp to Phe mutants, the homologous pair Trp68 and Trp156 were found to be extremely quenched, with quantum yields close to 0.01. The homologous pair Trp42 and Trp130 were moderately fluorescent, with quantum yields of 0.13 and 0.17, respectively. In an attempt to identify quenching and/or electrostatically perturbing residues, a set of 17 candidate amino acids around Trp68 and Trp156 were substituted with neutral or hydrophobic residues. None of these mutants showed significant changes in the fluorescence intensity compared to their own background. Hybrid quantum mechanical−molecular mechanical (QM-MM) simulations with the four different excited Trps as electron donors strongly indicate that electron transfer rates to the amide backbone of Trp68 and Trp156 are extremely fast relative to those for Trp42 and Trp130. This is in agreement with the quantum yields measured experimentally and consistent with the absence of a quenching side chain. Efficient electron transfer to the backbone is possible for Trp68 and Trp156 because of the net favorable location of several charged residues and the orientation of nearby waters, which collectively stabilize electron transfer electrostatically. The fluorescence emission spectra of single and double Trp to Phe mutants provide strong evidence for energy transfer from Trp42 to Trp68 in the N-terminal domain and from Trp130 to Trp156 in the C-terminal domain. The backbone conformation of tryptophans in Hγ D-Crys may have evolved in part to enable the lens to become a very effective UV filter, while the efficient quenching provides an in situ mechanism to protect the tryptophans of the crystallins from photochemical degradation.

The ∼30-fold variation of intrinsic Trp fluorescence intensity and lifetime in proteins is widely exploited to follow changes in protein structure such as folding/unfolding, substrate or ligand binding, and protein−protein interactions (*1*−*5*). The origin of weak Trp fluorescence in some proteins has long been believed to be due to electron transfer from excited Trp to an amide carbonyl group (*6*−*9*). Recent experiments affirm that the local backbone amides can be efficient quenchers in peptides (*10*) and in proteins (*11*). Other efficient amino acid electron transfer-based quenchers of Trp fluorescence are protonated His, Cys, disulfide, protonated Asp and Glu, and the amides of Asn and Gln (*12*−*17*). In addition, hydronium ion, Lys, and Tyr can quench Trp fluorescence by proton transfer (*12*, *18*). Met has also been implicated as a fluorescence quencher (*19*, *20*). An unusual NH···π hydrogen bond involving the indole nitrogen of the Trp and the benzene ring of a nearby Phe residue was also suggested to cause the Trp fluorescence quenching of FKBP59-1 (*21*, *22*) and human interleukin-2 (*23*). Nanda and Brand (*24*) proposed that an NH···π hydrogen bond between Trp48 and Phe8 in a homeodomain is responsible for the quenching of Trp48. However, the F8A mutant (*25*) still maintains low Trp fluorescence intensity, suggesting that the NH···π hydrogen bond was not responsible for Trp quenching in this homeodomain.

Despite these considerable investigations, a reliable understanding of when a particular quenching process will be exceptionally efficient in a protein has been elusive. A reasonable basis for the large Trp quantum yield variation using quantum mechanics−molecular mechanics (QM-MM)[1]

† Supported by National Institutes of Health Grant GM 17980 and NEI Grant EY 015834 (to J.K.) and NSF Grants MCB-0133064 and MCB-0446542 (to P.R.C.).

* Authors to whom correspondence should be addressed. Phone: (406) 994-5414 (P.R.C.); (617) 253-4700 (J.K.). Fax: (406) 994-5407 (P.R.C.); (617) 252-1843 (J.K.). E-mail: pcallis@montana.edu; jaking@mit.edu.

‡ Massachusetts Institute of Technology.

§ Montana State University.

[1] Abbreviations: Hγ D-Crys, human γD-crystallin; QM-MM, hybrid quantum mechanics−molecular mechanics; CT, charge transfer; GuHCl, guanidine hydrochloride; 3MI, 3-methylindole; ET, electron transfer; FRET, Förster resonance energy transfer; Ex, excitation.

10.1021/bi060988v CCC: $33.50
Published on Web 08/30/2006

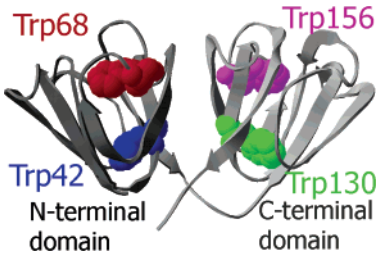

FIGURE 1: Ribbon structure of wild-type HγD-Crys showing Trp42 and Trp68 in the N-terminal domain and Trp130 and Trp156 in the C-terminal domain (PDB code 1HK0).

simulations has recently been presented (*26*−*30*). The method keys on the average energy and fluctuations of the lowest Trp ring-to-amide backbone charge transfer (CT)[1] state relative to the fluorescing state. The energy, fluctuations, and relaxation of normally high lying CT states are extremely sensitive to protein environment (local electric field direction and strength). Charged or polar environmental residues (including water) can either stabilize or destabilize the charge transfer and thus affect quantum yields (*26*, *27*, *31*). When the energy gap is large and fluctuations are small, the probability that the fluorescing and CT states will have the same energy is low. Electron transfer (the quenching process) is only possible when the fluorescing and CT states have the same energy.

The α-, β-, and γ-crystallins are the main protein components of the mammalian lens. The β- and γ-crystallins are structural proteins, while α-crystallin is a molecular chaperone and a structural protein (*32*, *33*). The oligomeric β- and the monomeric γ-crystallins have similar structures that contain four β-sheet Greek key motifs separated into two domains (*34*, *35*). Because there is no protein turnover in the lens, the crystallins have to remain soluble and stable throughout the human lifetime (*36*). Cataract, the leading cause of blindness worldwide (*37*, *38*), may be due to aggregation and deposition of partially unfolded crystallins (*39*). Cataracts removed from the human lens are composed of different species of aggregated crystallins, including covalently damaged human γD-crystallin (HγD-Crys)[1] (*40*). Oxidized forms of Trp156 in HγD-Crys have been identified from aged cataractous human lens by mass spectrometry (*41*).

HγD-Crys is a two-domain, 173 amino acid protein that is predominantly found in the lens nucleus (*36*). Mutations in the gene encoding HγD-Crys have been found to cause juvenile-onset cataract, supporting a role for HγD-Crys in cataractogenesis (*42*, *43*). The structure of the protein has been solved at 1.25 Å resolution by Basak et al. (*35*). This monomeric protein is composed of antiparallel β-sheets arranged in four Greek key motifs. The two domains show high levels of structural and sequence homology. HγD-Crys has four buried Trps at positions 42 and 68 in the N-terminal domain and positions 130 and 156 in the C-terminal domain (Figure 1).

HγD-Crys is considerably more fluorescent in the denatured state than in the native state, despite the absence of metal ligands or cofactors (*44*). Native state fluorescence quenching has also been observed for other β- and γ-crystallins (*45*, *46*). To investigate which Trps are involved in the quenching phenomenon, Kosinski-Collins et al. (*47*) constructed triple Trp mutants, each with three of the four endogenous Trps substituted with Phe. On the basis of the fluorescence spectra of the triple Trp mutants, it was found that Trp68 and Trp156 displayed extremely low fluorescence intensity, whereas Trp42 and Trp130 showed much higher fluorescence intensity (*47*).

Ultraviolet radiation is considered one of the risk factors for cataract formation (*48*). Although the cornea filters out almost all UV radiation of wavelengths shorter than 295 nm, the crystallin proteins within the lens are continuously exposed to ambient UV radiation of wavelengths longer than 295 nm throughout life (*49*). Photochemical reactions of Trps in the lens crystallins correlate with cataract formation (*50*, *51*). The photolysis reaction of UV-irradiated Trp may originate from the excited singlet state and may compete with fluorescence emission (*50*, *51*). The quenching of Trp fluorescence in HγD-Crys shortens the lifetime of the excited state and thus may minimize the chance of photoreaction and protect Trp residues from UV damage.

The fluorescence quantum yield ($\Phi_F = 0.040 \pm 0.005$) and the fluorescence decay rate of bovine γB-crystallin have been previously measured (*51*, *52*). Their study measured the total quantum yield of all four Trps of the protein, but it did not address their individual contributions. In this paper, we report the detailed quantitative measurement of the individual fluorescence emission spectra and the quantum yields of the four Trps in HγD-Crys. From characterization of single, double, and triple Trp mutants, partial Förster resonance energy transfer from the strongly (Trp42 and Trp130) to the weakly (Trp68 and Trp156) emitting Trp of the same domain was observed. A thorough search for a quenching residue through construction of mutants in different Trp backgrounds failed to identify plausible electron transfer to a neighboring residue. Similarly, substitution of charged and polar residues around Trp68 and Trp156 did not show a significant effect on the fluorescence intensities. The QM-MM simulations reported here decisively support highly efficient quenching by electron transfer from the excited Trp ring to its backbone amide as the reason for the weak fluorescence from Trp68 and Trp156. This is enabled by the large collective stabilization of the CT state by several charged residues and nearby waters.

MATERIALS AND METHODS

Mutagenesis, Expression, and Purification of Recombinant HγD-Crys. Primers encoding the substitutions described below (IDT-DNA) were used to amplify a pQE.1 plasmid encoding the HγD-Crys gene with an N-terminal 6-His tag (*47*). The single, double, and triple Trp to Phe substitutions (W42-only, W68-only, W130-only, and W156-only) were constructed by Kosinski-Collins et al. (*47*). Forty-one site-directed mutants in the different Trp backgrounds were constructed at 17 unique positions. These are summarized below in Figures 4 and 6 and Tables 2, 3, 6, 7, and 8. The mutants C32S, N33A, Y55F, Y62F, Y55F/Y62F, D64S, H65Q, Q66A, Q67A, M69S, D73S, and R79S were constructed in the W68-only background. The mutants H121Q, Y143F, Y150F, Y143F/Y150F, R152S, Y153Q, and D155S were constructed in the W156-only background. The mutants D64S, H65Q, M69S, D73S, and R79S were constructed in the W130F/W156F background. The mutants H121Q and Y153Q were constructed in the W42F/W68F background. The mutants D64S, H65Q, M69S, D73S, and R79S were

constructed in the W42F background. The mutant Y153Q was constructed in the W130F background. The mutants D64S, H65Q, M69S, D73S, R79S, H121Q, H65Q/H121Q, Y153Q, and R79S/Y153Q were constructed in the wild-type background. All of the mutations were confirmed by DNA sequencing (Massachusetts General Hospital).

The wild-type and mutant HγD-Crys proteins were expressed by *Escherichia coli* M15 [pREP4] cells. All of the mutants accumulated as native-like soluble proteins. The proteins were purified by affinity chromatography using a Ni-NTA resin (Qiagen) as previously described (*47*). The purities of the proteins were confirmed by SDS−PAGE.

Fluorescence Spectroscopy. The emission spectra of native proteins were recorded in S buffer (10 mM sodium phosphate, 5 mM DTT, 1 mM EDTA at pH 7.0). Buffer conditions for denatured proteins were S buffer plus 5.5 M guanidine hydrochloride (GuHCl).[1] Proteins were incubated in the denaturing buffer at 37 °C for 6 h prior to measuring fluorescence spectra. Concentrations of the wild-type and mutant His-tagged proteins were determined by measuring absorbance at 280 nm using extinction coefficients calculated with ProtParam (ExPASy). Fluorescence emission spectra were collected at 37 °C using a Hitachi F-4500 fluorescence spectrophotometer equipped with a circulating water bath. The band-pass for both excitation and emission was 10 nm. Intrinsic Trp fluorescence emission spectra of all the proteins were measured in the range of 310−420 nm using an excitation wavelength of 300 nm. A protein concentration of 1.38 μM was used for all experiments except for the quantum yield and energy transfer experiments. The protein concentrations used for experiments described in the Results section (see Resonance Energy Transfer between the Two Trps within Each Domain) were 2.75 μM. The buffer signal was subtracted from all spectra.

To measure how much the fluorescence intensity increased or decreased due to mutations in the different Trp backgrounds, the fluorescence emission spectra of native and unfolded proteins were recorded from three sets of samples prepared in parallel. The average value of the integrated fluorescence intensity was calculated, and signals of the native proteins were normalized for concentration by comparison with intensities of the unfolded protein spectra. The increase or decrease in quantum yields was calculated by comparing quantum yields of the mutants with those of their respective Trp backgrounds.

Quantum Yield Determinations. Quantum yields were calculated according to the equation:

$$Q = Q_R \left(\frac{I}{I_R}\right)\left(\frac{OD_R}{OD}\right)\left(\frac{n^2}{n_R^2}\right) \quad (1)$$

where Q and Q_R are the quantum yield of the protein and reference (L-Trp in water), I and I_R are the integrated fluorescence intensities of the protein and reference, OD and OD_R are the optical densities of the protein and reference at the excitation wavelength, and n and n_R are the refractive indices of the protein and reference solutions (*1*, *53*). The absolute quantum yield of Trp in water was taken to be 0.14 (*53*). The buffer for protein and Trp was S buffer at 37 °C. Quantum yields of the four Trps in HγD-Crys were measured using the proteins W42-only, W68-only, W130-only, and W156-only. Because there are 14 tyrosines in HγD-Crys, which may cause uncertainty in quantum yield measurements, an excitation wavelength of 300 nm was used in order to minimize tyrosine fluorescence. The emission spectra of wild-type HγD-Crys and the triple Trp mutants have maximal emission wavelengths that are close to the blue area (Table 1). There were significant portions of the blue edge of the emission spectra that could not be observed using a 300 nm excitation wavelength. We estimated the unobservable areas of the protein spectra by matching the longer wavelength areas of protein spectra with spectra of 3-methylindole (3MI)[1] in different solvent systems (see Supporting Information). The solvent system used to match 3MI spectra with the spectra of wild-type HγD-Crys was cyclohexane−dioxane (70:30), and the spectra of 3MI in cyclohexane−dioxane (83:17) were used to match the spectra of W42-only and W130-only. The spectra of 3MI in methanol−dioxane (25:75) were used to match the spectra of W68-only, and the spectra of 3MI in methanol−dioxane (10:90) were used to match the spectra of W156-only.

QM-MM Simulations. The hybrid QM-MM method used in this work has been described in recent publications (*26*−*30*) for applications to Trp fluorescence quenching in proteins. The method grew from an earlier QM-MM procedure used to predict the fluorescence wavelengths of Trp in proteins (*31*). Briefly, the QM method is Zerner's INDO/S-CIS method (*54*), modified to include the local electric fields and potentials at the atoms. The MM part is Charmm (version 26b) (*55*). Hydrogens were added to the crystal structure (PDB code 1HK0), and the entire protein was solvated within a 30 Å radius sphere of TIP3 explicit water. The waters were held within the 30 Å radius with a quartic potential. The quantum mechanical part includes the selected Trp and the amide of the preceding residue, capped with hydrogens, *N*-formyltryptophanamide. The electric potential due to all non-QM atoms in the protein and solvent is calculated with a dielectric constant = 1 for each QM atom and added to the QM Hamiltonian.

RESULTS

Fluorescence Emission Spectra and Quantum Yields. Fluorescence emission spectra of native and denatured wild-type HγD-Crys and the important Trp to Phe mutants are shown in Figures 2 and 3. An excitation wavelength of 300 nm was used in order to minimize tyrosine fluorescence. Instrument settings were the same for all spectra such that the areas under the curves are proportional to quantum yields. Figure 2A compares fluorescence spectra of native and denatured double and triple Trp mutants that give fluorescence only from Trps in the N-terminal domain (Trps 42 and/or 68). Figure 2B does the same for the C-terminal domain (Trps 130 and/or 156). Figure 3A compares native and denatured wild type and single mutants of the weakly emitting Trps (W68F and W156F). Figure 3B does the same for the strongly emitting Trps (W42F and W130F).

Figure 2 shows that the fluorescence from Trps 68 and 156 is extremely weak compared to that of Trps 42 and 130. The maximal emission wavelength for Trps 68 and 156 is red shifted approximately 10 nm compared to Trp42 and Trp130, consistent with a somewhat more polar environment for the former (Trps 68 and 156). The integrated intensities

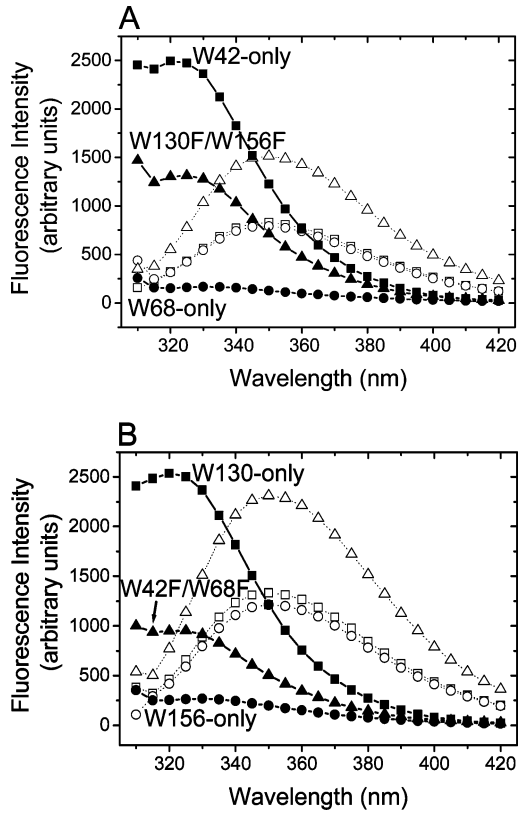

FIGURE 2: (A) Fluorescence emission spectra of native W42-only (■), W68-only (●), and W130F/W156F (▲) and denatured W42-only (□), W68-only (○), and W130F/W156F (△). (B) Fluorescence emission spectra of native W130-only (■), W156-only (●), and W42F/W68F (▲) and denatured W130-only (□), W156-only (○), and W42F/W68F (△). The solid lines represent the emission spectra of native proteins, and the dotted lines represent the unfolded proteins. An excitation wavelength of 300 nm was used for samples of 2.75 μM protein at 37 °C. Native proteins were incubated in S buffer, and unfolded proteins were incubated in S buffer plus 5.5 M GuHCl for 6 h at 37 °C before the measurements. The buffer signal was subtracted from all spectra.

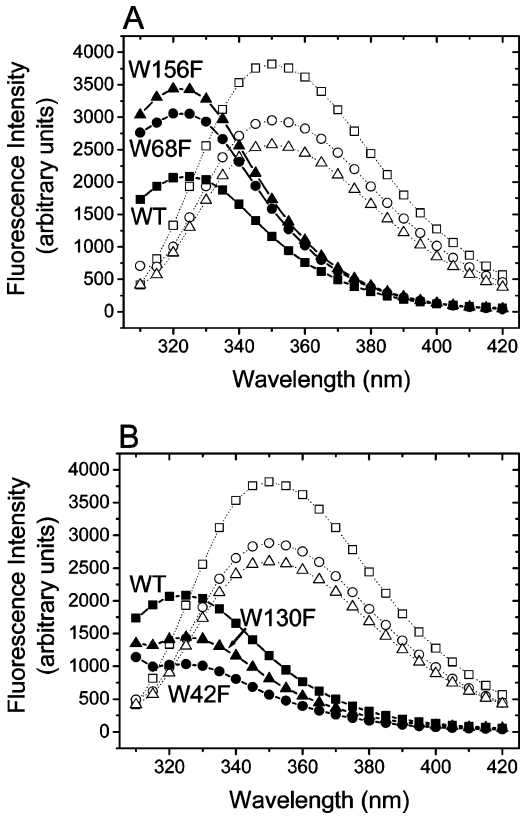

FIGURE 3: (A) Fluorescence emission spectra of native wild type (WT) (■), W68F (●), and W156F (▲) and denatured wild type (□), W68F (○), and W156F (△). (B) Fluorescence emission spectra of native wild type (■), W42F (●), and W130F (▲) and denatured wild type (□), W42F (○), and W130F (△). The solid lines represent the emission spectra of native proteins, and the dotted lines represent the unfolded proteins. An excitation wavelength of 300 nm was used for samples of 2.75 μM protein at 37 °C. Native proteins were incubated in S buffer, and unfolded proteins were incubated in S buffer plus 5.5 M GuHCl for 6 h at 37 °C before recording emission. The buffer signal was subtracted from all spectra.

of the fluorescence emission spectra of the unfolded proteins are approximately proportional to the number of Trps (Figures 2 and 3), suggesting that the environments of the four Trps become approximately the same in the denatured state.

Quantitative determinations of the quantum yields for wild type and the triple mutants are shown in Table 1. The quantum yields for Trp42 and Trp130 were found to be nearly 20 times higher than those of Trp68 and Trp156. The average quantum yield for the triple mutants is 0.080, somewhat higher than that of the wild type, which is 0.058.

Resonance Energy Transfer between the Two Trps within Each Domain. The fluorescence spectra in Figures 2 and 3 for single, double, and triple Trp mutants provide convincing evidence for intradomain Förster resonance energy transfer (FRET),[1] with the donor being the more fluorescent Trp in each domain (Trp42 in the N-terminal domain and Trp130 in the C-terminal domain). When Trp68 or Trp156 was individually substituted with Phe, the integrated fluorescence intensity of W68F was 38% higher than wild type and the integrated fluorescence intensity of W156F was 52% higher than wild type (Figure 3A). In contrast, the integrated fluorescence intensities of W42F and W130F decreased 50% and 29% compared to wild type, respectively (Figure 3B). These observations are consistent with Trp42 and Trp130 acting as energy donors. A considerable fraction of the excitation energy is not emitted because it is transferred to the weakly emitting partner. Because Trp42 and Trp130 make the major contributions to the overall fluorescence intensity of wild-type HγD-Crys, substituting them with Phe caused a decrease in fluorescence intensity (Figure 3B).

Table 1: Maximum Fluorescence Emission Wavelengths and Quantum Yields of Wild-Type and Triple Trp Mutants

protein	maximum Em wavelength (nm)	quantum yield
wild type	326	0.058 ± 0.006
W42-only	322	0.13 ± 0.01
W68-only	335	0.0076 ± 0.0008
W130-only	322	0.17 ± 0.02
W156-only	332	0.0099 ± 0.001

Fluorescence emission spectra of double Trp mutants were measured, and the results further support FRET. Fluorescence intensity of the double mutant W130F/W156F revealed the interaction of Trp42 and Trp68 in the N-terminal domain. Fluorescence intensity of this mutant did not equal the simple addition of W42-only and W68-only fluorescence but was instead about 43% lower than the intensity of W42-only and 6 times higher than the intensity of W68-only

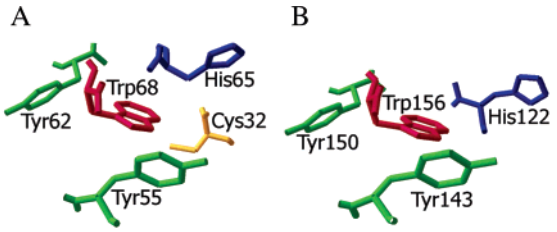

FIGURE 4: Crystal structure of Cys and Tyr-His-Tyr aromatic cages surrounding Trp68 (A) and Trp156 (B) (PDB code 1HK0).

(Figure 2A). A similar result was found for the mutant W42F/W68F, which revealed the interaction between Trp130 and Trp156 in the C-terminal domain (Figure 2B). The intensity of W42F/W68F was 59% lower than the intensity of W130-only and 3 times higher than W156-only.

Comparison of the spectrum of the double Trp mutant W42F/W68F (containing Trps 130 and 156) in Figure 2B with the single Trp mutant W42F (containing Trps 130, 156, and 68) in Figure 3B shows that there is no significant energy transfer from the highly fluorescent Trp130 in the C-terminal domain to the weakly fluorescent Trp68 in the N-terminal domain. If there is interdomain energy transfer from Trp130 to Trp68, the fluorescence intensity of the double Trp mutant W42F/W68F (containing Trps 130 and 156 but not potential energy acceptor Trp68) should be higher than the single Trp mutant W42F (containing Trps 130, 156, and 68). Because the fluorescence intensities of W42F/W68F and W42F are very similar, there is probably little or no interdomain energy transfer from Trp130 to Trp68. Similarly, the comparison of the double Trp mutant W130F/W156F (containing Trps 42 and 68) in Figure 2A and single Trp mutant W130F (containing Trps 42, 68, and 156) in Figure 3B shows that there is little or no energy transfer from Trp42 in the N-terminal domain to Trp156 in the C-terminal domain.

Investigation of Nearby Side Chain Contributions to Trp Quenching. Quenching of the buried Trp68 and Trp156 in HγD-Crys could be due to immediate interaction with the side chains of nearby amino acids (*12*). In the original γ-crystallin structure paper, Wistow et al. (*56*) proposed that interaction between the aromatic residues and neighboring cysteines or methionines may contribute to stability of the γ-crystallin structure. The contributions of nearby residues around Trp68 and Trp156 to fluorescence quenching were determined by substitution with neutral or hydrophobic residues. The residues mutated were a cysteine nearby Trp68 and the Tyr-His-Tyr triads around both Trp68 and Trp156 (Figure 4, Tables 2 and 3).

In aqueous solution, cysteine strongly quenches Trp fluorescence by excited-state electron transfer, apparently during collisions (*12*). The distance between the SH group of Cys32 and the C6 of Trp68 is 3.9 Å, suggesting that Cys32 could be a potential quencher of Trp68 (*51*, *52*). However, compared to the fluorescence intensity of W68-only, the mutant C32S/W68-only did not show a significant increase in fluorescence intensity (Table 2).

Previous inspection suggested that the Tyr-His-Tyr aromatic "cage" surrounding Trp68 and Trp156 may be the source of native state quenching (*47*). To test whether the tyrosine residues quenched fluorescence by proton transfer (*12*), the emission spectra of six tyrosine mutants have been characterized. None of the mutants displayed a significant increase or decrease in fluorescence intensity (variance <10%) compared to the spectra of W68-only or W156-only (Figure 4 and Table 2). On the basis of the triple Trp background, single tyrosine mutants (Y55F/W68-only, Y62F/W68-only, Y143F/W156-only, and Y150F/W156-only) did not show effects on the fluorescence intensities compared to their background. Therefore, the double tyrosine mutants (Y55F/Y62F/W68-only and Y143F/Y150F/W156-only) were further constructed. It is possible that, in the single tyrosine mutants, the other unchanged tyrosine in the aromatic cage may extensively quench Trp fluorescence and obscure the effect of the single tyrosine substitutions. The double tyrosine mutants did not display an increase in fluorescence, thus ruling out this possibility.

Histidine in its protonated form is another common fluorescence "quencher" via electron transfer (*13*, *16*, *17*, *57*). Fluorescence spectra of the mutants H65Q, H65Q/W68-only, H65Q/W130F/W156F, H121Q, H121Q/W156-only, H121Q/W42F/W68F, and H65Q/H121Q were recorded and compared to their respective Trp backgrounds (Tables 2 and 3). The double mutant H65Q/H121Q was studied to investigate whether there is an additive quenching effect of these two histidines. Except for H65Q/W68-only and H121Q/W156-only, none of the mutants displayed an increase in native fluorescence intensity. However, the increases of H65Q/W68-only and H121Q/W156-only represent insignificant variations in quantum yield magnitude (Table 2). Previous equilibrium unfolding and refolding experiments demonstrated that HγD-Crys was destabilized by the triple Trp substitutions (*47*). We have found that the mutant H65Q has a destabilized N-terminal domain and H121Q has a

Table 2: Quantum Yields of the Mutants of Nearby Side Chains Surrounding Trp68 and Trp156 in the Triple Trp to Phe Substitution Background

protein	quantum yield[a]
W68-only	**0.0076**
C32S/W68-only	−0.0002[c]
H65Q/W68-only	+0.0058[b]
Y55F/W68-only	+0.0003
Y62F/W68-only	+0.0002
Y55F/Y62F/W68-only	+0.0002
W156-only	**0.0099**
H121Q/W156-only	+0.0022
Y143F/W156-only	−0.0002
Y150F/W156-only	−0.0005
Y143F/Y150F/ W156-only	−0.0008

[a] Standard derivations of quantum yields for all proteins were less than ±10% of their absolute quantum yield values. [b] (+) represents an increase in quantum yield of the mutants compared to their background. [c] (−) represents a decrease in quantum yield of the mutants compared to their background.

Table 3: Quantum Yields of His to Gln Mutants Surrounding Trp68 and Trp156 in the Wild-Type or Double Trp to Phe Substitution Background

protein	quantum yield[a]	protein	quantum yield[a]
wild type	**0.058**	**W130F/W156F**	**0.034**
H65Q	+0.001[b]	H65Q/W130F/W156F	+0.0003
H121Q	+0.001	**W42F/W68F**	**0.024**
H65Q/H121Q	+0.002	H121Q/W42F/W68F	+0.0008

[a] Standard derivations of quantum yields for all proteins were less than ±10% of their absolute quantum yield values. [b] (+) represents an increase in quantum yields of the mutants compared to their background.

Table 4: Computed Energy Differences, Electron Transfer Rates, and Quantum Yields

residue	CT-^1L_a gap (kilo·cm^{-1})	std dev (kilo·cm^{-1})	ET rate constant ($\times 10^7$ s^{-1})	predicted quantum yield
Trp42	5.2	1.7	86.3	0.040
Trp68	0.34	2.5	1180	0.003
Trp130	6.0	1.6	32.9	0.087
Trp156	1.0	2.6	1040	0.004
Trp42 (vacuum)	6.6	1.0	2.4	0.259
Trp68 (vacuum)	8.4	0.5	0.0000	0.308
Trp130 (vacuum)	8.5	0.6	0.0000	0.308
Trp156 (vacuum)	11.0	0.7	0.0000	0.308

destabilized C-terminal domain (data not shown). Therefore, the fluorescence intensity increases of H65Q/W68-only and H121Q/W156-only are probably due to slight conformational changes or partial unfolding caused by the high number of mutations.

QM-MM Estimates of Relative Fluorescence Quantum Yields. Using the same parameters and procedures as described previously (*26*), QM-MM simulations were carried out for HγD-Crys. The results are in accord with the experimental observations. Table 4 shows the average CT-^1L_a energy gap, the standard deviation of this gap, the computed electron transfer rate, and the predicted fluorescence quantum yield for each of the four Trps. The calculations predict Trp68 and Trp156 to be very weakly fluorescent and Trp42 and Trp130 to be moderately fluorescent. The detailed differences between experiment and theory are within the accuracy of the method.

The order of magnitude difference in the quantum yields between the two pairs of Trps arises primarily from the much larger energy gap and smaller fluctuation of the gap for Trp42 and Trp130. When the energy gap is large and fluctuations are small, the probability that the fluorescing and CT states will have the same energy is low. Electron transfer (the quenching process) is only possible when the fluorescing and CT states have the same energy. For Trp68 and Trp156, the CT state is much more stabilized by the local protein electrostatic environment, resulting in an electron transfer (ET)[1] rate much faster than the natural deactivation rate and, therefore, a much reduced quantum yield.

For Trp68 and Trp156, the lowest CT state has an electron transferred from the indole ring primarily to the π^* molecular orbital of the Trp backbone amide. Most of the transferred electron density is centered on the C, with minor amounts on the O and N. A net positive charge is distributed on several atoms of the indole ring. Therefore, the CT state energy is quite sensitive to the strength and direction of the average electric field in the direction of electron transfer. Positive charges near the amide C and/or negative charges near the indole ring will lower the energy (stabilize), and the opposite case will raise the energy. Charged residues lying on a line perpendicular to the dipole of the CT state will have little effect. Hydrogen bonds donated to the amide carbonyl are a powerful source of CT state stabilization, and polar residues (including waters) near the indole ring will stabilize, destabilize, or have little effect on the CT state depending on the orientation of the dipole relative to the ET direction.

Because of the reasonably long-range nature of Coulombic interaction energies involved (inverse distance squared for ion−dipole and inverse distance cubed for dipole−dipole), the net stabilization is a relatively small number derived from the sum of many large positive and negative terms. For example, Table 5 lists Coulombic contributions to the CT-^1L_a energy gap from charged and uncharged protein residues, close waters, distant waters, and totals for Trp68 and Trp42. The difference in each category is also listed.

Table 5: Shifts of the CT-^1L_a Energy Gap Due to the Protein and Water Environment for Trp42 and Trp68[a]

source	Trp68	Trp42	difference	Trp156	Trp130	difference
Lys	0.99	2.66	−1.67	−0.13	−0.45	0.31
Arg	0.96	−4.77	5.72	4.02	8.51	−4.49
Asp	−6.75	−1.76	−4.98	−0.10	−0.92	0.81
Glu	−1.50	−1.17	−0.33	−6.58	−8.94	2.35
Gly1	0.63	−0.49	1.12	−0.15	−1.07	0.91
Ser173	−0.12	0.93	−1.05	−0.13	0.51	−0.64
charged	−5.79	−4.60	−1.19	−3.09	−2.35	−0.74
noncharged	0.74	1.09	−0.35	−2.84	0.91	−3.75
all protein	−4.55	−3.07	**−1.48**	−6.21	−1.99	**−4.22**
all water	−3.82	2.08	**−5.91**	−4.07	0.55	**−4.61**
wat <9 Å	−6.64	−1.59	−5.06	−4.18	0.75	−4.93
wat >9 Å	2.82	3.67	−0.85	0.11	−0.20	0.32
protein + water	−8.37	−0.99	**−7.38**	−10.28	−1.44	**−8.83**

[a] Energy contributions are in units of kilo·cm^{-1} (1 kilo·cm^{-1} = 0.125 eV = 2.9 kcal/mol). Negative values mean stabilization of the CT state relative to ^1L_a.

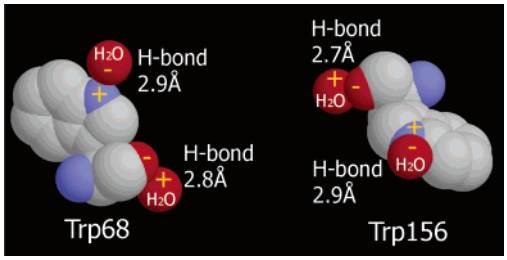

FIGURE 5: Interaction between Trp68 (or Trp156) and the two nearby crystallographic waters, which will stabilize the electron transfer from the indole ring to the amide backbone (PDB code 1HK0).

As shown in Table 5, the average contributions from charged groups are large and quite different for Trp68 and Trp42, a reflection of positioning of the groups relative to the direction of electron transfer. The total average contribution from the protein is large and negative, with Trp68 being stabilized overall by 1480 cm^{-1} more than Trp42. A much larger effect comes from the water molecules, for which the CT state of Trp68 is stabilized by 3820 cm^{-1} while that of Trp42 is *destabilized* by 2080 cm^{-1}. Overall, the average CT state stabilization of Trp68 is 7380 cm^{-1} greater than for Trp42. The single most dominating reason for the much greater quenching rate of Trp68 is the presence of ca. 10 waters on average within 9 Å that stabilize the CT state by 6640 cm^{-1}. For Trp42 there are only about three waters within 9 Å, and these only stabilize by about 1600 cm^{-1} on average.

Two crystallographic waters present in the X-ray crystal structure (*35*) are close to the quenched Trps and appear to be highly stabilizing for electron transfer (Figure 5). One water molecule donates an H-bond to the Trp backbone CO (the electron acceptor). The proximity of the positive charge of the H to the backbone CO group stabilizes the charge transfer state. The other water molecule is an H-bond

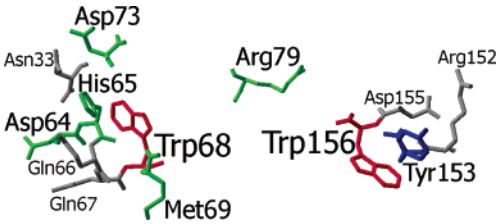

FIGURE 6: Charged and polar residues around Trp68 and Trp156 that were mutated (PDB code 1HK0).

acceptor from the Trp indole NH. This H-bond places the negative charge of the O near the Trp ring (the electron donor) to further stabilize the charge transfer state.

In addition to the external electrostatic perturbations from protein and water molecules, the internal electronic energy depends somewhat on the precise local conformation of the Trp and its associated amides. Of considerable importance is the distance between the electron acceptor and donor groups and the stabilization of these through proximity of the polar atoms of the amides within the QM unit. Table 4 also shows the CT-^1L_a average energy gap and standard deviation for the QM fragments in a vacuum. The gap for Trp68 is similar to that for many other proteins previously studied, but that for Trp42 is somewhat smaller. For this reason, the predicted quantum yield for Trp42 is not as high as normally expected when the environment stabilization is as small as found for this Trp.

Much the same summary picture is found for Trp130 and Trp156, although many details are different because the two domains are not identical. The stabilization difference between the Trp156 and Trp130 CT states is somewhat greater than the difference between Trp68 and Trp42. This is brought about by much more protein stabilization, moderated by less water stabilization for the Trp156−Trp130 pair than for the Trp68−Trp42 pair.

Investigation of the Stabilization Effect of Charged and Polar Side Chains on the Charge Transfer State. A subset of site-directed mutants were constructed and analyzed to test the effect of charged or polar residues on the charge transfer state. These were chosen on the basis of the QM-MM results described above.

In the X-ray crystal structure of HγD-Crys, the polar or charged residues Asn33, Asp64, His65, Gln66, Gln67, Met69, and Asp73 are in proximity to Trp68. Arg152, Tyr153, and Asp155 are nearby Trp156 (Figure 6). QM-MM results predicted that Arg79 highly stabilizes and Tyr153 destabilizes the charge transfer event of Trp156 (see Supporting Information). To experimentally investigate their contributions to electron transfer, neutral and polar amino acid substitutions of these residues were constructed to test their role in stabilizing the charge transfer state (Tables 6−8). On the basis of the triple Trp mutant background, D64S, H65Q, D73S, R79S, and Y153Q showed more than 30% increase in fluorescence intensity. Q67A, M69S, and R152S showed about 20% increase in fluorescence intensity. Because of the extremely weak fluorescence from the triple mutants, W68-only or W156-only, these increases are very small on the scale of absolute quantum yield increase (Table 6).

As explained above for H65Q, we were concerned that these increases were due to subtle conformational changes or partial unfolding because of the high numbers of mutations (*47*). To confirm this, the substitutions of D64S, H65Q, M69S, D73S, R79S, and Y153Q were also constructed in the wild-type and double Trp backgrounds (Table 7), which

Table 6: Effect of Mutations on Fluorescence Intensity by Affecting Charge Transfer States (in the Triple Trp to Phe Substitution Background)

protein	quantum yield[a]
W68-only	**0.0076**
N33A/W68-only	+0.0008[b]
Q66A/W68-only	+0.0009
Q67A/W68-only	+0.0017
D64S/W68-only	+0.0024
H65Q/W68-only	+0.0058
M69S/W68-only	+0.0019
D73S/W68-only	+0.0047
R79S/W68-only	+0.0038
W156-only	**0.0099**
R152S/W156-only	+0.0027
D155S/W156-only	−0.0001[c]
Y153Q/W156-only	+0.0039

[a] Standard derivations of quantum yields for all proteins were less than ±10% of their absolute quantum yield values. [b](+) represents an increase in quantum yields of the mutants compared to their background. [c] (−) represents a decrease in quantum yields of the mutants compared to their background.

Table 7: Effect of Mutations on Fluorescence Intensity by Affecting Charge Transfer States (in the Wild-Type or Double Trp to Phe Substitution Background)

protein	quantum yield[a]
wild type	**0.058**
D64S	−0.0001[c]
H65Q	+0.001[b]
M69S	+0.0003
D73S	+0.0002
R79S	+0.0001
Y153Q	+0.010
W130F/W156F	**0.034**
D64S/W130F/W156F	+0.0003
H65Q/W130F/W156F	+0.0003
M69S/W130F/W156F	−0.0001
D73S/W130F/W156F	+0.003
R79S/W130F/W156F	+0.0005
W42F/W68F	**0.024**
Y153Q/W42F/W68F	+0.010

[a] Standard derivations of quantum yields for all proteins were less than ±10% of their absolute quantum yield values. [b] (+) represents an increase in quantum yields of the mutants compared to their background. [c] (−) represents a decrease in quantum yields of the mutants compared to their background.

Table 8: Effect of Mutations on Fluorescence Intensity by Affecting Charge Transfer States (in the Single Trp to Phe Substitution Background)

protein	quantum yield[a]
W42F	**0.029**
D64S/W42F	+0.0003[b]
H65Q/W42F	−0.001[c]
M69S/W42F	+0.001
D73S/W42F	+0.001
R79S/W42F	−0.001
W130F	**0.041**
Y153Q/W130F	+0.005

[a] Standard derivations of quantum yields for all proteins were less than ±10% of their absolute quantum yield values. [b] (+) represents an increase in quantum yields of the mutants compared to their background. [c](−) represents a decrease in quantum yields of the mutants compared to their background.

were more thermodynamically stable than the triple Trp mutants. The double Trp background was constructed by maintaining two Trps in each domain. Except for Y153Q, which showed a slight increase in fluorescence intensity, none of other substitutions displayed an increase in fluorescence intensity in the wild-type or double Trp backgrounds. There was no obvious difference in fluorescence intensities for the mutants in these more stable backgrounds (Table 7). The mutants D64S, H65Q, M69S, D73S, and R79S displayed fluorescence intensity increases in the triple Trp background that were probably due to subtle conformation change or partial unfolding caused by the high number of substitutions.

Asp73 was predicted to be one of the strongest enhancers for the charge transfer process (see Supporting Information). Asp64 may also stabilize the charge transfer complex, but less effectively than Asp73. The calculations predicted that the R79S mutant might cause an increase in fluorescence because Arg79 lies on the direction of electron transfer. The electron is transferred toward Arg79, and so the charge transfer state will be stabilized more than if a neutral residue were in this position. Because the distance from Arg79 to Trp68 or Trp156 is more than 10 Å, without theoretical calculations, we did not test Arg79 in our initial survey of neighboring charged and polar amino acids. However, by the experimental measures, none of these substitutions showed significant effects on the fluorescence intensity. Possible reasons for the failure of these predictions are presented in the Discussion (see Charge Transfer Mechanism).

Arg152 and Asp155 were predicted to have little effect on the quantum yield of Trp156 because they lie in a line perpendicular to the direction of electron transfer. Consistent with this prediction, the fluorescence intensity of the mutants R152S and D155S did not increase significantly.

As described above, we have observed FRET between the two Trps of each domain. The interaction between the Trps may obscure the effect of the substitutions of these potential charge transfer enhancers. In other words, even if the mutants in the wild-type or double Trp background did destabilize the charge transfer complex and increase the fluorescence intensity of Trp68 or Trp156, there may be more energy transfer from Trp42 or Trp130. If this were the case, we would not see changes in fluorescence intensity.

To rule out this possibility the single Trp substitutions W42F and W130F were constructed to eliminate the interaction between Trp42 and Trp68 in the N-terminal domain and the interaction between Trp130 and Trp156 in the C-terminal domain (Table 8). Trp42 and Trp130 are also sensitive to the electrostatic mutations, and therefore their fluorescence intensity may change and obscure the substitution effect. None of the substitutions caused an increase in fluorescence intensity in the W42F mutant background as compared to the background fluorescence intensity of W42F. Y153Q/W130F showed about 10% fluorescence intensity increase (quantum yield increases 0.005) compared to the W130F background.

DISCUSSION

Understanding the mechanisms of the quenching of tryptophan fluorescence in proteins is technically important for a variety of experiments in which the Trp's fluorescence serves as a reporter of protein conformation and protein−protein and protein−ligand interactions. In the case of the crystallins, which are subject to decades of light exposure, the quenching may reflect evolved physiological functions of the proteins.

Trp to Trp Energy Transfer. Resonance energy transfer between aromatic amino acids often occurs in proteins due to the absorption and emission spectra overlap of Phe, Tyr, and Trp (*1*). We consider whether the observations attributed to FRET in HγD-Crys are physically reasonable. The distance between the indole rings of two Trps of the N-terminal domain is 12.2 Å, and the distance between Trps of the C-terminal domain is 12.4 Å. These distances are within the range (4−16 Å) of typical Förster distances (the distance for which the probability of transfer is 50%) for energy transfer between Trps (*1*). In contrast, the distances between the Trps in different domains are more than 20 Å, so the possibility of the interdomain Trp energy transfer is very low. The experimental results are consistent with this. For significant transfer, the emission spectrum of the donor must overlap the absorption spectrum of the acceptor. Although we were not able to directly determine the extent of this overlap because of light scattering by the protein solutions, a reasonable basis for expecting favorable overlap for energy transfer in the direction observed comes from the excitation and fluorescence spectra of 3MI in the solvent mixtures used to emulate the fluorescence spectra of the triple mutants shown in Figure 2. The fluorescence spectrum of 3MI in cyclohexane−dioxane (83:17) has a maximum at 322 nm, which closely matches those of Trps 42 and 130 at wavelengths >315 nm. The fluorescence spectra of 3MI in methanol−dioxane (25:75 and 10:90) have maxima near 335 nm, which closely match those of Trps 68 and 156, respectively, at wavelengths >315 nm (see Supporting Information). The overlap of the excitation spectrum in the more polar solvent (methanol−dioxane) with the emission spectrum in the less polar solvent (cyclohexane−dioxane) is found to be an order of magnitude higher than the reverse (the overlap of the excitation spectrum in the less polar solvent with the emission spectrum in the more polar solvent). This behavior is much more pronounced when the two solvents are pure cyclohexane and pure butanol. These observations are completely consistent with the observation that energy transfer is from the Trps with the blue-shifed fluorescence spectra (Trps 42 and 130) to those with the red-shifted fluorescence spectra (Trps 68 and 156).

The remaining factor for efficient transfer is the orientation factor κ^2, which is a function of the average relative orientation of the transition dipole vectors of the donor and acceptor during the excited state lifetime. Its value can range from 0 to 4. It is 2 when the vectors are parallel side by side, and 4 if parallel end-to-end, but goes through 0 when parallel and tilted at 54 deg to the line connecting the donor and acceptor. κ^2 is $^2/_3$ when the chromophores are tumbling rapidly and randomly during the excited state lifetime. In the present protein environment, κ^2 is expected to be approximately constant but could vary because of the deformations of the protein structure. Tabulated experimental and computed transition dipole directions for the $^1L_a \rightarrow$ ground state transition for indole place the direction approximately between the line connecting atoms CE3 and NE3 and the line connecting atoms CE3 and CD1 of the indole

ring (*58*). Using the coordinates from 50 frames of a molecular dynamics simulation at 300 K gave $\kappa^2 = 0.4 \pm 0.2$ and 0.5 ± 0.2 for transfer from Trp42 and Trp130, respectively. In summary, all three critical factors are probably large enough to allow the extent of partial transfer observed.

Applying Förster theory to the crystal structure of bovine γB-crystallin, Borkman (*59*) predicted that the efficiency of energy transfer from the protein's 15 tyrosines to the 4 Trps would be approximately 83%. This prediction agreed well with the experimental value of 78% (*59*). Although there are no previous reports of Trp-to-Trp energy transfer in the β- or γ-crystallins, homotransfer between Trps has been observed in other proteins. For example, in barnase there is energy transfer from Trp71 to Trp94, and Trp94 is in turn quenched by His18 (*13*, *57*). On the basis of the distance between the Trps in bovine γB-crystallin (>12 Å), Borkman et al. (*51*) predicted that Trp-to-Trp energy transfer would not be possible in this protein. However, our experimental observations and theoretical considerations give a clear indication of partial transfer.

Charge Transfer Mechanism. As in earlier papers (*26*), the quantum yields were estimated here with electron transfer theory that has a universal electron transfer matrix element of $V = 10$ cm^{-1} and a universal offset of $D = -4000$ cm^{-1} from the computed energy gap. Thus, all quantum yields reflect only the adjusted average CT-^1L_a energy gap and the standard deviation of this gap. The gap is modulated by the net electric potential difference between the initial electron distribution and that in the CT state. We are working on a more realistic model wherein the magnitude of V is computed.

It is interesting that the quantum yields for the pairs Trps 68/156 and Trps 42/130 are similar. While this might be expected given the similar homology in the two domains, especially regarding the positions of the Trps, inspection of Tables 4 and 5 shows that the individual terms contributing to computed energy gaps differ considerably between the homologous Trps, even though the net result is quite similar CT-^1L_a energy gaps and standard deviations. Table 5 also shows that the detailed backbone conformations differ considerably, as judged by the average gap in a vacuum.

The method successfully captures the essence of the quantum yield behavior, predicting extremely low values for Trp68 and Trp156 and intermediate values for Trp42 and Trp130. The highest fluorescence yields for single Trps in proteins are typically around 0.3, a value that varies only slightly with the polarity of the environment. The computations even correctly predict that Trp130 is more fluorescent than Trp42 and Trp156 more than Trp68, although this is likely fortuitous given that all are a factor of 2−3 too low.

One of the important outcomes of this study is the testing of detailed predictions of the theoretical method by strategic mutations. Using a variant of the program that computes the average energy gap, contributions of individual residues and waters to the CT-^1L_a gap for each Trp were determined (see Supporting Information). Large contributions come from five sources: (1) charged residues that lie on the axis of electron transfer; (2) backbone atom contributions from nearby residues; (3) hydrogen bonding from very close waters; (4) dipole−dipole interactions from near waters; and (5) collective contributions from distant waters that are aligned by the charged groups of the protein. Contributions for the charged groups are predicted to be large at long range if lying on the electron transfer direction axis. For example, Arg79 stabilizes the CT state for Trp156 by 2000 cm^{-1} even though 21 Å distant. On the basis of such calculations we anticipated that mutations of these charged residues to neutral residues would have an observable impact on the energy gap and thus measurably affect the quantum yield. However, as noted in the Results section, replacement of the candidate charged residues with neutral residues failed to produce significant changes in quantum yield.

A more thorough consideration provides the likely reason for these negative results. First, every charged group has an orienting effect on the water, creating a collective dipole that opposes the direct effect of the charge on the CT state. Because charged groups are almost always on the surface, their effect on water is large. This is merely the microscopic manifestation of the large dielectric constant of water, which the simulations capture reasonably well. A more subtle effect comes from the fact that the more fluorescent Trps are also sensitive to electrostatic mutations. For example, Arg79 stabilizes the CT state of Trp130 by 1500 cm^{-1}, i.e., almost as much as it stabilizes Trp156. Furthermore, because the quantum yield is a sigmoidal function of the energy gap, Trps such as 130 and 42 that fluoresce with about half the maximum possible efficiency are more sensitive to the electric field than those which are at the top or bottom (flatter regions) of the curve (*29*). Therefore, changes in response to mutating away the charge of Arg79 are expected to be dominated by increased fluorescence from Trp130, if present. Another problem with mutating charges is that very often they are part of ion pairs. Removal of a charge may result in unpredictable repositioning of other charged groups, facilitated by the large, flexible nature of Lys, Arg, and Glu.

In water, cysteine is a powerful quencher of the indole ring by electron transfer and has been implicated as a quencher in some proteins. The ineffectiveness of Cys32 as a quencher of Trp68 fluorescence, despite the S being only 4 Å from some ring atoms, is probably because the electrostatic factors are destabilizing. Electron transfer to Cys32 would be in the opposite direction from that to the amide (which is highly stabilized). Part of the reason for the amide CT stabilization is the high density of negative atoms in the vicinity of the Cys32 S.

The Potential Physiological Role for Lens UV Absorption in Protecting the Retina. Ultraviolet radiation is often classified into three bands based on their biological effects: UVA (400-320 nm), UVB (320−290 nm), and UVC (290−100 nm). Under normal conditions, the ozone layer filters out all UVC and 90% of UVB light and thus prevent them from reaching the earth's surface (*60*). The cornea can absorb almost all of the UV radiation of wavelength shorter than 295 nm. However, significant radiation of wavelengths longer than 300 nm pass the cornea (*61*). The young crystallin lens absorbs the remaining UVB and UVA light of wavelengths below 370 nm. When the lens becomes more yellow with age, its UV absorption spectrum expands to include wavelengths up to 470 nm (*48*, *62*).

People who have had surgical removal of a cataract are sensitive to UV radiation (*61*, *63*−*66*). This sensitivity of the retina to UV radiation in the absence of the lens has been shown in animal models (*67*, *68*). These observations

indicate that one function of the lens is to protect the retina from UV light that is transmitted by cornea. We suspect that one function of the highly conserved tryptophans in the crystallin proteins is to absorb UV reaching the lens, to protect the retina. The lens also contains low molecular weight molecules which may also act as UV filters protecting the retina, such as kynurenine and 3-hydroxykynureine (*69*, *70*).

Does Fluorescence Quenching Protect the Crystallins from UV Photodamage? Exposure to UV radiation not only causes damage to the retina photoreceptors (*71*) but also is an important risk factor for cataract formation (*49*). Though only limited intensities of UVB and UVA light of wavelengths between 295 and 400 nm reach the lens, the cumulative exposure to ambient UV over decades may be significant in cataract formation (*60*). UVB at 300 nm was most detrimental to the lens in the animal models (*72*, *73*). Trp absorption at 300 nm is the tail of the tryptophan UV absorption curve but is still the most significant source of UV absorption at this wavelength in proteins (*1*).

Trp radical formation and fluorescent material derived from Trps have been identified in lens exposed to UV light with wavelengths longer than 295 nm (*74*−*76*). The excited singlet state Trps may then be photochemically degraded via photoionization reactions, which result in indole ring cleavage (*77*−*79*). Trp residues (as well as His, Met, and Cys) were photochemically reactive in UV-irradiated bovine γB-crystallin (*80*). Such UV-induced Trp radical formation may play an important role in senile cataract formation (*74*−*76*).

Ultraviolet irradiation of bovine crystallins resulted in protein aggregation (*81*−*83*). HγD-Crys also aggregates upon UV irradiation (Abigail Bushman and Jonathan King, unpublished results). The direct covalent product of UV photodamage to the tryptophans has the indole ring opened, generating the Trp radical cation (*78*, *84*, *85*). This introduction of a charge into the buried hydrophobic core of the γ-crystallins would be expected to be partially denaturing (*80*). Partially unfolded species are the precursor of aggregation and fibril formation during in vitro refolding of HγD-Crys (*44*). We suspect that partially unfolded species generated by cleavage of the indole ring are also the precursors to further protein aggregation.

Tallmadge and Borkman (*86*) studied Trp's damage in bovine γB-crystallin irradiated in vitro at 295 nm with 0.7 mW/cm^2 output flux. Their results showed that the rates of photolysis of Trp42 and Trp131 were much higher than Trp68 and Trp157. The structures of bovine γB-crystallin and HγD-Crys are highly homologous, and their four Trps are conserved (*39*, *87*). We have shown that Trp42 and Trp130 are moderately fluorescent and Trp68 and Trp156 are extensively quenched in HγD-Crys. This suggests that quenching of Trp68 and Trp157 may protect Trps from photodamage.

Pitts et al. (*88*) have established threshold levels of exposure throughout the near-UV region (210−440 nm) for cataract formation in rabbits. For instance, the threshold dose at 295 nm was 0.75 J·cm^{-2} and was 0.15 J·cm^{-2} at 300 nm. These results are on the same order as the maximum tolerable dose at 300 nm (0.365 J·cm^{-2}) measured in the rat (*73*). Borkman (*89*) suggested a photon-to-Trp ratio of 20:1 to cause Trp destruction by estimates of the Trp photolysis yield in solution.

If the crystallins are absorbing incident UV radiation, fluorescence quenching of Trps may be a self-protective mechanism from damage induced by UV radiation. Photochemical reaction of Trp probably originates from excited singlet states and competes with fluorescence emission (*51*). Quenching can shorten the lifetime of Trp excited singlet states, perhaps reducing the possibility that the electron will go into a photochemical reaction. The highly quenched Trp68 and Trp156 may function as "energy sinks". Our findings strongly suggest that energy from the ambient UV absorbed by these two Trps is almost completely dissipated through nonradiative quenching and therefore the chance of a photodamage reaction may be reduced. It remains to be determined whether the quenching phenomenon in HγD-Crys is conserved though other crystallin proteins. If so, this would suggest that the backbone conformation of Trps in HγD-Crys may have evolved to provide efficient absorption of UVB radiation, while at the same time providing maximum protection from photodamage.

CONCLUSION

Trps 68 and 156 of HγD-Crys display abnormally low fluorescence intensity in the native state without the existence of the metal ligands or cofactors. An extensive investigation of mutated proteins combined with hybrid quantum mechanical−molecular mechanical (QM-MM) simulations strongly implicates efficient electron transfer from the excited indole ring to the backbone amide of these residues. Charged residues and nearby waters favorably stabilize these charge transfer events. Considerable resonance energy transfer from Trp42 to Trp68 in the N-terminal domain and from Trp130 to Trp156 in the C-terminal domain was observed and rationalized. The energy transfer to the weakly fluorescing Trps (Trp68 and Trp156) serves to further reduce the overall quantum yield (and presumably excited state lifetime) of HγD-Crys. We speculate that this quenching may protect Trps in γ-crystallins from UV-induced photodamage and reflect an evolved property of the crystallin fold.

SUPPORTING INFORMATION AVAILABLE

Tables (1S−8S) showing residues that stabilize or destabilize four Trps in HγD-Crys and figures (1S−10S) showing the fluorescence emission spectra of 3MI and the spectra of triple Trp mutants (W42-only, W68-only, W130-only, and W156-only) for the extrapolation of the quantum yields of four Trps in HγD-Crys on the blue side. This material is available free of charge via the Internet at http://pubs.acs.org.

REFERENCES

1. Lakowicz, J. (1999) *Principles of fluorescence spectroscopy*, 2nd ed., Kluwer Academic/Plenum, New York.
2. Beechem, J. M., and Brand, L. (1985) Time-resolved fluorescence of proteins, *Annu. Rev. Biochem. 54*, 43−71.
3. Eftink, M. R. (1991) Fluorescence techniques for studying protein structure, *Methods Biochem. Anal. 35*, 127−205.
4. Smirnov, A. V., English, D. S., Rich, R. L., Lane, J., Teyton, L., Schwabacher, A. W., Luo, S., Thornburg, R. W., and Petrich, J. W. (1997) Photophysics and biological applications of 7-azaindole and its analogs, *J. Phys. Chem. B 101*, 2758−2769.
5. Prendergast, F. G. (1991) Time-resolved fluorescence techniques: methods and applications in biology, *Curr. Opin. Struct. Biol. 1*, 1054−1059.

6. Cowgill, R. W. (1963) Fluorescence and the structure of proteins. I. Effects of substituents on the fluorescence of indole and phenol compounds, *Arch. Biochem. Biophys. 100*, 36−44.
7. Chang, M. C., Petrich, J. W., McDonald, D. B., and Fleming, G. R. (1983) Nonexponential fluorescence decay of tryptophan, tryptophylglycine, and glycyltryptophan, *J. Am. Chem. Soc. 105*, 3819−3824.
8. Colucci, W. J., Tilstra, L., Sattler, M. C., Fronczek, F. R., and Barkley, M. D. (1990) Conformational studies of a constrained tryptophan derivative: implications for the fluorescence quenching mechanism, *J. Am. Chem. Soc. 112*, 9182−9190.
9. Chen, Y., Liu, B., Yu, H.-T., and Barkley, M. D. (1996) The peptide bond quenches indole fluorescence, *J. Am. Chem. Soc. 118*, 9271−9278.
10. Pan, C. P., Callis, P. R., and Barkley, M. D. (2006) Dependence of tryptophan emission wavelength on conformation in cyclic hexapeptides, *J. Phys. Chem. B 110*, 7009−7016.
11. Sillen, A., Hennecke, J., Roethlisberger, D., Glockshuber, R., and Engelborghs, Y. (1999) Fluorescence quenching in the DsbA protein from Escherichia coli: complete picture of the excited-state energy pathway and evidence for the reshuffling dynamics of the microstates of tryptophan, *Proteins 37*, 253−263.
12. Chen, Y., and Barkley, M. D. (1998) Toward understanding tryptophan fluorescence in proteins, *Biochemistry 37*, 9976−9982.
13. Loewenthal, R., Sancho, J., and Fersht, A. R. (1991) Fluorescence spectrum of barnase: contributions of three tryptophan residues and a histidine-related pH dependence, *Biochemistry 30*, 6775−6779.
14. Weisenborn, P. C. M., Meder, H., Egmond, M. R., Visser, T. J., and Hoek, A. (1996) Photophysics of the single tryptophan residue in Fusarium solani cutinase: Evidence for the occurrence of conformational substates with unusual fluorescence behaviour, *Biophys. Chem. 58*, 281−288.
15. Hennecke, J., Sillen, A., Huber-Wunderlich, M., Engelborghs, Y., and Glockshuber, R. (1997) Quenching of tryptophan fluorescence by the active-site disulfide bridge in the DsbA protein from Escherichia coli, *Biochemistry 36*, 6391−6400.
16. Harris, D. L., and Hudson, B. S. (1990) Photophysics of tryptophan in bacteriophage T4 lysozymes, *Biochemistry 29*, 5276−5285.
17. Harris, D. L., and Hudson, B. S. (1991) Fluorescence and molecular dynamics study of the internal motion of the buried tryptophan in bacteriophage T4 lysozyme: Effects of temperature and alteration of nonbonded networks, *Chem. Phys. 158*, 353−382.
18. Vander, D. E. (1969) Fluorescence solvent shifts and singlet excited state pK's of indole derivatives, *Bull. Soc. Chim. Belg. 78*, 69−75.
19. Kuznetsova, I. M., and Turoverov, K. K. (1998) What determines the characteristics of the intrinsic UV-fluorescence of proteins? Analysis of the properties of the microenvironment and features of the localization of their tryptophan residues, *Tsitologiia 40*, 747−762.
20. Yuan, T., Weljie, A. M., and Vogel, H. J. (1998) Tryptophan fluorescence quenching by methionine and selenomethionine residues of calmodulin: orientation of peptide and protein binding, *Biochemistry 37*, 3187−3195.
21. Rouviere, N., Vincent, M., Craescu, C. T., and Gallay, J. (1997) Immunosuppressor binding to the immunophilin FKBP59 affects the local structural dynamics of a surface beta-strand: time-resolved fluorescence study, *Biochemistry 36*, 7339−7352.
22. Craescu, C. T., Rouviere, N., Popescu, A., Cerpolini, E., Lebeau, M. C., Baulieu, E. E., and Mispelter, J. (1996) Three-dimensional structure of the immunophilin-like domain of FKBP59 in solution, *Biochemistry 35*, 11045−11052.
23. Nanda, V., Liang, S. M., and Brand, L. (2000) Hydrophobic clustering in acid-denatured IL-2 and fluorescence of a Trp NH-pi H-bond, *Biochem. Biophys. Res. Commun. 279*, 770−778.
24. Nanda, V., and Brand, L. (2000) Aromatic interactions in homeodomains contribute to the low quantum yield of a conserved, buried tryptophan, *Proteins 40*, 112−125.
25. Subramaniam, V., Jovin, T. M., and Rivera-Pomar, R. V. (2001) Aromatic amino acids are critical for stability of the bicoid homeodomain, *J. Biol. Chem. 276*, 21506−21511.
26. Callis, P., and Liu, T. (2004) Quantitative predictions of fluorescence quantum yields for tryptophan in proteins., *J. Phys. Chem. B 108*, 4248−4259.
27. Callis, P., and Vivian, J. (2003) Understanding the variable fluorescence quantum yield of tryptophan in proteins using QM-MM simulations. Quenching by charge transfer to the peptide backbone, *Chem. Phys. Lett. 369*, 409−414.
28. Kurz, L. C., Fite, B., Jean, J., Park, J., Erpelding, T., and Callis, P. (2005) Photophysics of tryptophan fluorescence: link with the catalytic strategy of the citrate synthase from Thermoplasma acidophilum, *Biochemistry 44*, 1394−1413.
29. Liu, T., Callis, P. R., Hesp, B. H., de Groot, M., Buma, W. J., and Broos, J. (2005) Ionization potentials of fluoroindoles and the origin of nonexponential tryptophan fluorescence decay in proteins, *J. Am. Chem. Soc. 127*, 4104−4113.
30. Xu, J., Toptygin, D., Graver, K. J., Albertini, R. A., Savtchenko, R. S., Meadow, N. D., Roseman, S., Callis, P. R., Brand, L., and Knutson, J. R. (2006) Ultrafast fluorescence dynamics of tryptophan in the proteins monellin and IIA(Glc), *J. Am. Chem. Soc. 128*, 1214−1221.
31. Vivian, J. T., and Callis, P. R. (2001) Mechanisms of tryptophan fluorescence shifts in proteins, *Biophys. J. 80*, 2093−2109.
32. Horwitz, J. (1992) Alpha-crystallin can function as a molecular chaperone, *Proc. Natl. Acad. Sci. U.S.A. 89*, 10449−10453.
33. Singh, K., Groth-Vasselli, B., Kumosinski, T. F., and Farnsworth, P. N. (1995) alpha-Crystallin quaternary structure: molecular basis for its chaperone activity, *FEBS Lett. 372*, 283−287.
34. Lapatto, R., Nalini, V., Bax, B., Driessen, H., Lindley, P. F., Blundell, T. L., and Slingsby, C. (1991) High resolution structure of an oligomeric eye lens beta-crystallin. Loops, arches, linkers and interfaces in beta B2 dimer compared to a monomeric gamma-crystallin, *J. Mol. Biol. 222*, 1067−1083.
35. Basak, A., Bateman, O., Slingsby, C., Pande, A., Asherie, N., Ogun, O., Benedek, G. B., and Pande, J. (2003) High-resolution X-ray crystal structures of human gammaD crystallin (1.25 Å) and the R58H mutant (1.15 Å) associated with aculeiform cataract, *J. Mol. Biol. 328*, 1137−1147.
36. Oyster, C. (1999) *The human eye: strucutre and function. Chapter 12. The lens and the vitreous*, Sinauer Associates, Sunderland, MA.
37. Hyman, L. (1987) Epidemiology of eye disease in the elderly, *Eye 1* (Part 2), 330−341.
38. Rahmani, B., Tielsch, J. M., Katz, J., Gottsch, J., Quigley, H., Javitt, J., and Sommer, A. (1996) The cause-specific prevalence of visual impairment in an urban population. The Baltimore Eye Survey, *Ophthalmology 103*, 1721−1726.
39. Bloemendal, H., de Jong, W., Jaenicke, R., Lubsen, N. H., Slingsby, C., and Tardieu, A. (2004) Ageing and vision: structure, stability and function of lens crystallins, *Prog. Biophys. Mol. Biol. 86*, 407−485.
40. Hanson, S. R., Hasan, A., Smith, D. L., and Smith, J. B. (2000) The major in vivo modifications of the human water-insoluble lens crystallins are disulfide bonds, deamidation, methionine oxidation and backbone cleavage, *Exp. Eye Res. 71*, 195−207.
41. Searle, B. C., Dasari, S., Wilmarth, P. A., Turner, M., Reddy, A. P., David, L. L., and Nagalla, S. R. (2005) Identification of protein modifications using MS/MS de novo sequencing and the OpenSea alignment algorithm, *J. Proteome Res. 4*, 546−554.
42. Pande, A., Pande, J., Asherie, N., Lomakin, A., Ogun, O., King, J. A., Lubsen, N. H., Walton, D., and Benedek, G. B. (2000) Molecular basis of a progressive juvenile-onset hereditary cataract, *Proc. Natl. Acad. Sci. U.S.A. 97*, 1993−1998.
43. Nandrot, E., Slingsby, C., Basak, A., Cherif-Chefchaouni, M., Benazzouz, B., Hajaji, Y., Boutayeb, S., Gribouval, O., Arbogast, L., Berraho, A., Abitbol, M., and Hilal, L. (2003) Gamma-D crystallin gene (CRYGD) mutation causes autosomal dominant congenital cerulean cataracts, *J. Med. Genet. 40*, 262−267.
44. Kosinski-Collins, M. S., and King, J. (2003) In vitro unfolding, refolding, and polymerization of human gammaD crystallin, a protein involved in cataract formation, *Protein Sci. 12*, 480−490.
45. Kim, Y. H., Kapfer, D. M., Boekhorst, J., Lubsen, N. H., Bachinger, H. P., Shearer, T. R., David, L. L., Feix, J. B., and Lampi, K. J. (2002) Deamidation, but not truncation, decreases the urea stability of a lens structural protein, betaB1-crystallin, *Biochemistry 41*, 14076−14084.
46. Wenk, M., Herbst, R., Hoeger, D., Kretschmar, M., Lubsen, N. H., and Jaenicke, R. (2000) Gamma S-crystallin of bovine and human eye lens: solution structure, stability and folding of the intact two-domain protein and its separate domains, *Biophys. Chem. 86*, 95−108.
47. Kosinski-Collins, M. S., Flaugh, S. L., and King, J. (2004) Probing folding and fluorescence quenching in human gammaD crystallin Greek key domains using triple tryptophan mutant proteins, *Protein Sci. 13*, 2223−2235.

48. Oliva, M. S., and Taylor, H. (2005) Ultraviolet radiation and the eye, *Int. Ophthalmol. Clin. 45*, 1−17.
49. Colitz, C. M., Bomser, J. A., and Kusewitt, D. F. (2005) The endogenous and exogenous mechanisms for protection from ultraviolet irradiation in the lens, *Int. Ophthalmol. Clin. 45*, 141−155.
50. Kurzel, R. B., Wolbarsht, M., Yamanashi, B. S., Staton, G. W., and Borkman, R. F. (1973) Tryptophan excited states and cataracts in the human lens, *Nature 241*, 132−133.
51. Borkman, R. F., Douhal, A., and Yoshihara, K. (1993) Picosecond fluorescence decay of lens protein gamma-II crystallin, *Biophys. Chem. 47*, 203−211.
52. Mandal, K., Bose, S. K., Chakrabarti, B., and Siezen, R. J. (1985) Structure and stability of gamma-crystallins. I. Spectroscopic evaluation of secondary and tertiary structure in solution, *Biochim. Biophys. Acta 832*, 156−164.
53. Chen, R. (1967) Fluorescence quantum yields of tryptophan and tyrosine, *Anal. Lett. 1*, 35−42.
54. Ridley, J., and Zerner, M. (1973) An intermediate neglect of differential overlap technique for spectroscopy: Pyrrole and the azines, *Theor. Chim. Acta (Berlin) 32*, 111−134.
55. MacKerell, A. D., Bashford, D., Bellott, M., Dunbrack, R. L., Evanseck, J. D., Field, M. J., Fischer, S., Gao, J., Guo, H., Ha, S., Joseph-McCarthy, D., Kuchnir, L., Kuczera, K., Lau, F. T. K., Mattos, C., Michnick, S., Ngo, T., Nguyen, D. T., Prodhom, B., Reiher, W. E., Roux, B., Schlenkrich, M., Smith, J. C., Stote, R., Straub, J., Watanabe, M., Wiórkiewicz-Kuczera, J., Yin, D., and Karplus, M. (1998) All-atom empirical potential for molecular modeling and dynamics studies of proteins, *J. Phys. Chem. B 102*, 3586−3616.
56. Wistow, G., Turnell, B., Summers, L., Slingsby, C., Moss, D., Miller, L., Lindley, P., and Blundell, T. (1983) X-ray analysis of the eye lens protein gamma-II crystallin at 1.9 Å resolution, *J. Mol. Biol. 170*, 175−202.
57. Willaert, K., Loewenthal, R., Sancho, J., Froeyen, M., Fersht, A., and Engelborghs, Y. (1992) Determination of the excited-state lifetimes of the tryptophan residues in barnase, via multifrequency phase fluorometry of tryptophan mutants, *Biochemistry 31*, 711−716.
58. Callis, P. R. (1997) ^1L_a and ^1L_b transitions of tryptophan: applications of theory and experimental observations to fluorescence of proteins, *Methods Enzymol. 278*, 113−150.
59. Borkman, R. F., and Phillips, S. R. (1985) Tyrosine-to-tryptophan energy transfer and the structure of calf gamma-II crystallin, *Exp. Eye Res. 40*, 819−826.
60. McCarty, C. A., and Taylor, H. R. (2002) A review of the epidemiologic evidence linking ultraviolet radiation and cataracts, in *Progress in Lens and Cataract Research* (Hockwin, O., Kojima, M., Takahashi, N., and Sliney, D. H., Eds.) pp 21−31, Karger, Basel.
61. Lerman, S. (1980) *Radiant energy and the eye. Chapter 3: Biological and chemical effects of ultraviolet radiation*, Macmillan, New York.
62. Lerman, S. (1987) Chemical and physical properties of the normal and aging lens: spectroscopic (UV, fluorescence, phosphorescence, and NMR) analyses, *Am. J. Optom. Physiol. Opt. 64*, 11−22.
63. Liu, I. Y., White, L., and LaCroix, A. Z. (1989) The association of age-related macular degeneration and lens opacities in the aged, *Am. J. Public Health 79*, 765−769.
64. Berler, D. K., and Peyser, R. (1983) Light intensity and visual acuity following cataract surgery, *Ophthalmology 90*, 933−936.
65. Pollack, A., Marcovich, A., Bukelman, A., and Oliver, M. (1996) Age-related macular degeneration after extracapsular cataract extraction with intraocular lens implantation, *Ophthalmology 103*, 1546−1554.
66. Pollack, A., Bukelman, A., Zalish, M., Leiba, H., and Oliver, M. (1998) The course of age-related macular degeneration following bilateral cataract surgery, *Ophthalmic Surg. Lasers 29*, 286−294.
67. Ham, W. T., Jr., Mueller, H. A., Ruffolo, J. J., Jr., Guerry, D., III, and Guerry, R. K. (1982) Action spectrum for retinal injury from near-ultraviolet radiation in the aphakic monkey, *Am. J. Ophthalmol. 93*, 299−306.
68. Noell, W. K., Walker, V. S., Kang, B. S., and Berman, S. (1966) Retinal damage by light in rats, *Invest. Ophthalmol. 5*, 450−473.
69. Streete, I. M., Jamie, J. F., and Truscott, R. J. (2004) Lenticular levels of amino acids and free UV filters differ significantly between normals and cataract patients, *Invest. Ophthalmol. Visual Sci. 45*, 4091−4098.
70. Hood, B. D., Garner, B., and Truscott, R. J. (1999) Human lens coloration and aging. Evidence for crystallin modification by the major ultraviolet filter, 3-hydroxy-kynurenine O-beta-D-glucoside, *J. Biol. Chem. 274*, 32547−32550.
71. Massof, R., Sykes, S., Rapp, L., Robison, W., Zwick, H., and Hochheimer, B. (1986) Optical radiation damage to the ocular photoreceptors, in *Optical radiation and visual health* (Waxler, M., and Hitchins, V., Eds.) Chapter 4, pp 69−88, CRC Press, Boca Raton, FL.
72. Merriam, J. C., Lofgren, S., Michael, R., Soderberg, P., Dillon, J., Zheng, L., and Ayala, M. (2000) An action spectrum for UV-B radiation and the rat lens, *Invest. Ophthalmol. Visual Sci. 41*, 2642−2647.
73. Soderberg, P. G., Lofgren, S., Ayala, M., Dong, X., Kakar, M., and Mody, V. (2002) Toxicity of ultraviolet radiation exposure to the lens expressed by maximum tolerable dose, in *Progress in lens and cataract research.* (Hockwin, O., Kojima, M., Takahashi, N., and Sliney, D. H., Eds.) pp 70−75, Karger, Basel.
74. Borkman, R. F. (1977) Ultraviolet action spectrum for tryptophan destruction in aqueous solution, *Photochem. Photobiol. 26*, 163−166.
75. Lerman, S., and Borkman, R. (1978) Ultraviolet radiation in the aging and cataractous lens. A survey, *Acta Ophthalmol. (Copenhagen) 56*, 139−149.
76. Weiter, J. J., and Finch, E. D. (1975) Paramagnetic species in cataractous human lenses, *Nature 254*, 536−537.
77. Feitelson, J. (1971) The formation of hydrated electrons from the excited state of indole derivatives, *Photochem. Photobiol. 13*, 87−96.
78. Bryant, F. D., Santus, R., and Grosswelner, L. I. (1975) Laser flash photolysis of aqueous tryptophan, *J. Phys. Chem. 79*, 2711−2716.
79. Templer, H., and Thistlethwaite, P. J. (1976) Flash photolysis of aqueous tryptophan, alanyl tryptophan and tryptophyl alanine, *Photochem. Photobiol. 23*, 79−83.
80. Hott, J. L., and Borkman, R. F. (1992) Analysis of photo-oxidized amino acids in tryptic peptides of calf lens gamma-II crystallin, *Photochem. Photobiol. 56*, 257−263.
81. Raman, B., and Rao, C. M. (1994) Chaperone-like activity and quaternary structure of alpha-crystallin, *J. Biol. Chem. 269*, 27264−27268.
82. Hott, J. L., and Borkman, R. F. (1993) Concentration dependence of transmission losses in UV-laser irradiated bovine alpha-, beta H-, beta L- and gamma-crystallin solutions, *Photochem. Photobiol. 57*, 312−317.
83. Walker, M. L., and Borkman, R. F. (1989) Light scattering and photocrosslinking in the calf lens crystallins gamma-II, III and IV, *Exp. Eye Res. 48*, 375−383.
84. Tallmadge, D. H., Huebner, J. S., and Borkman, R. F. (1989) Acrylamide quenching of tryptophan photochemistry and photophysics, *Photochem. Photobiol. 49*, 381−386.
85. Hibbard, L. B., Kirk, N. J., and Borkman, R. F. (1985) The effect of pH on the aerobic and anaerobic photolysis of tryptophan and some tryptophan-containing dipeptides, *Photochem. Photobiol. 42*, 99−106.
86. Tallmadge, D. H., and Borkman, R. F. (1990) The rates of photolysis of the four individual tryptophan residues in UV exposed calf gamma-II crystallin, *Photochem. Photobiol. 51*, 363−368.
87. Srikanthan, D., Bateman, O. A., Purkiss, A. G., and Slingsby, C. (2004) Sulfur in human crystallins, *Exp. Eye Res. 79*, 823−831.
88. Pitts, D. G., Cullen, A. P., Hacker, P. D., and Parr, W. H. (1977) Ocular ultraviolet effects from 295 nm to 400 nm in the rabbit eye, in pp. (NIOSH) Publ. No. 77-175, U.S. Department of Health, Education and Welfare, Washington, DC.
89. Borkman, R. F. (1984) Cataracts and photochemical damage in the lens, *Ciba Found. Symp. 106*, 88−109.

BI060988V